Hot-carrier relaxation in CdSe/CdS core/shell nanoplatelets

Matthew Pelton,[1,2,] Yana Wang,[3] Igor Fedin,[4,†] Dmitri V. Talapin,[2.4] and Stephen K. O'Leary[3]*

[1] Department of Physics, UMBC (University of Maryland, Baltimore County), Baltimore, MD 21250, U.S.A.

[2] Center for Nanoscale Materials, Argonne National Laboratory, Argonne, IL 60439, U.S.A.

[3] School of Engineering, The University of British Columbia, Kelowna, British Columbia V1V 1V7, Canada

[4] Department of Chemistry and James Franck Institute, University of Chicago, Chicago, IL 60637, U.S.A.

ABSTRACT. Understanding the relaxation of high-energy carriers in two-dimensional semiconductor nanomaterials is critical for development of applications based on these materials. Colloidal CdSe/CdS core/shell nanoplatelets provide an outstanding model system for investigations of these relaxation dynamics. Here, we present time-resolved photoluminescence spectroscopy of a series of nanoplatelets with different core and shell thicknesses. For times between 10 ps and 1 ns and for shell thicknesses up to 4 monolayers, the measured carrier relaxation dynamics are well described by a simple model of Auger reheating: biexcitonic Auger recombination continually increases the average energy of the carriers (while decreasing their number), and this reheating sets a bottleneck to cooling through electron-phonon coupling. For times between 1 and 10 ps, the relaxation dynamics are consistent with electron-phonon coupling, where the bottleneck is now the decay of the LO-phonon population. For shell thicknesses greater than 4 monolayers, the simple Auger-reheating model cannot quantitatively explain the measurement results.

KEYWORDS. Nanoplatelets, two-dimensional materials, carrier relaxation, carrier cooling, Auger recombination, CdSe, core/shell

Relaxation of carriers in semiconductor nanomaterials from high-energy states within the conduction and valence bands down to the band-edge states plays an important role in the potential optoelectronic applications of the materials. For example, rapid relaxation is favorable for light-emitting devices,[1] so that band-edge emitting states are quickly filled, and high-energy carriers are not lost to traps. On the other hand, slow relaxation is favorable for extraction of high-energy carriers, enabling the hot carriers to be used for photocatalysis,[2] or in hot-carrier solar cells.[3] Relaxation dynamics are determined both by the intrinsic properties of the materials that make up nanostructures as well as the size and shape of the nanostructures. The dimensionality of carrier confinement plays an especially important role in determining their relaxation dynamics in nanostructures; in particular, quasi-two-dimensional (quantum-well) nanostructures exhibit qualitatively different carrier-relaxation properties than quasi-zero-dimensional (quantum-dot) nanostructures.[4]

II-VI semiconductor nanoplatelets (NPLs),[5] or colloidal quantum wells, have multiple properties that make them outstanding model systems for experimental studies of relaxation dynamics in two-dimensional semiconductors.[6] Perhaps most important is that they can be synthesized colloidally with atomic-level monodispersity in their thicknesses, providing bulk samples with nearly zero inhomogeneous broadening. In addition, shells of different semiconductor materials can be grown epitaxially on the nanoplatelets using solution-phase techniques that preserve this single-monolayer monodispersity, enabling relaxation dynamics to be probed in highly controlled heterostructures.

We have previously examined relaxation dynamics in CdSe NPLs[7] and found that they were dominated by the effects of Auger recombination.[8] Specifically, we showed that the continuous density of states and rapid internal thermalization meant that the carrier energy distribution can be

described in terms of an instantaneous temperature, $T(t)$, that decreases from a high initial value (determined by the amount of optical energy absorbed by an NPL) to a lower temperature through exchange of heat with the crystal lattice; this is in contrast with the sequential relaxation through discrete states that is characteristic of quantum dots.[9] However, at the same time as the carriers cool, they are undergoing biexcitonic Auger recombination, which has been shown to dominate recombination dynamics in CdSe NPLs and in CdSe/CdS core/shell nanoplatelets,[10,11] This means that the carriers are constantly re-heated at the same time as they cool: the biexcitonic Auger process involves one exciton recombining by transferring its energy to a second exciton, and the excess energy of the second exciton is rapidly redistributed among the other excitons in the NPL. The competition provided by this reheating sets the time scale of carrier cooling.[12] The Auger-reheating mechanism has also been observed to govern carrier relaxation dynamics in CdSe nanorods[13] and metal halide perovskites,[14,15,16] and is thus of broad interest in the development of optoelectronic nanomaterials.

Here, we systematically study carrier relaxation on picosecond to nanosecond time scales in CdSe/CdS core/shell NPLs with a range of core and shell thicknesses. We find that the Auger reheating mechanism dominates relaxation dynamics for shell thicknesses up to 4 monolayers (ML) and for time scales greater than approximately 10 ps. For shorter time scales and for thicker CdS shells, the data cannot be described by a simple model of Auger-reheating dynamics.

Results

Auger-Limited Recombination Dynamics

In our previous work, we showed that biexcitonic Auger recombination dominates the recombination dynamics in CdSe NPLs and in CdSe/CdS core/shell nanoplatelets.[10] The primary

evidence for this is that measurements of time-resolved photoluminescence (PL) are consistent with the expectation for a two-exciton recombination process:

$$\frac{dN(t)}{dt} = -A[N(t)]^2, \quad (1)$$

where $N(t)$ is the average number of excitons in a nanoplatelet at time, and A is a constant that determines the rate of Auger recombination. This description based on a continuous differential equation has been shown to be a good approximation for $N(t) > 2$.[17]

Here, we present a new analysis of the previous data based on this same rate equation. Specifically, we adapt the "inversion analysis" method of Ref. 18 to our time-resolved PL measurements. The CdSe/CdS core/shell NPLs that we study are synthesized as described in Ref. 10, following Refs. 4 and 19. Time-resolved PL measurements are also performed as described in Ref. 10. Briefly, a dilute solution of NPLs is excited with a pulsed laser at a wavelength of 400 nm, and emitted light is resolved as a function of wavelength and as a function of time after excitation using a streak camera with a grating-spectrometer attachment. The total PL intensity as a function of time delay is obtained by integrating measured PL spectra for each time delay after excitation over the range of wavelengths that corresponds to the PL peak from the NPLs. The background due to dark counts is then determined by averaging over all negative time delays, and this value is subtracted from the measured data for all time delays.

The resulting time-dependent total PL intensity, $I(t)$, is proportional to $N(t)$. According to Eq. (1), then, a double-logarithmic plot of $-dI(t)/dt$ as a function of $I(t)$ should give a straight line with a slope of 2. Producing such a plot requires numerical differentiation of $I(t)$; if this differentiation is done directly on the experimental data, the measurement noise will be amplified

and will obscure the results. We therefore follow Ref. 18 and smooth the data by fitting to a multiexponential function; it is important to note that this multiexponential fit is done simply to reduce experimental noise and does not have any physical significance. The smoothed data can then be differentiated numerically, resulting in a smoothed plot.

Figure 1a shows representative results. The plot is shown in terms of $N(t)$ and $-dN(t)/dt$, using the scaling between $N(t)$ and $I(t)$ based on our time-shift analysis (described below); however, this scaling simply affects the x- and y-axis scales equally, and does not affect the slope of the line on the double-logarithmic plot. Figure 1a also shows a fit to a straight line with a slope of 2, as expected for biexcitonic Auger recombination dynamics, showing good agreement for $N > 2$. Deviations are seen for $N < 1.5$; this is expected, because at least two excitons must be present in any given NPL in order for Auger recombination to be possible.

The only adjustable parameter in this fit is the offset, which is equal to the Auger recombination rate, *A*. The values of *A* obtained by this analysis can be compared to the values that we obtain by the "time-shift" analysis that we developed in Refs. 10 and 8. In this analysis, we combine the $I(t)$ data obtained for different excitation pump fluences by shifting each of the traces along the time axis so that they fall on top of one another. At low fluences, the curves fall on top of one another without being shifted in time; this corresponds to fluences for which one or less exciton is excited, on average, into each NPL. The maximum fluence for which this is the case is used to determine the point at which the average exciton population, $N(t) = 1$, and this point is used to calibrate the proportionality factor between $N(t)$ and $I(t)$.

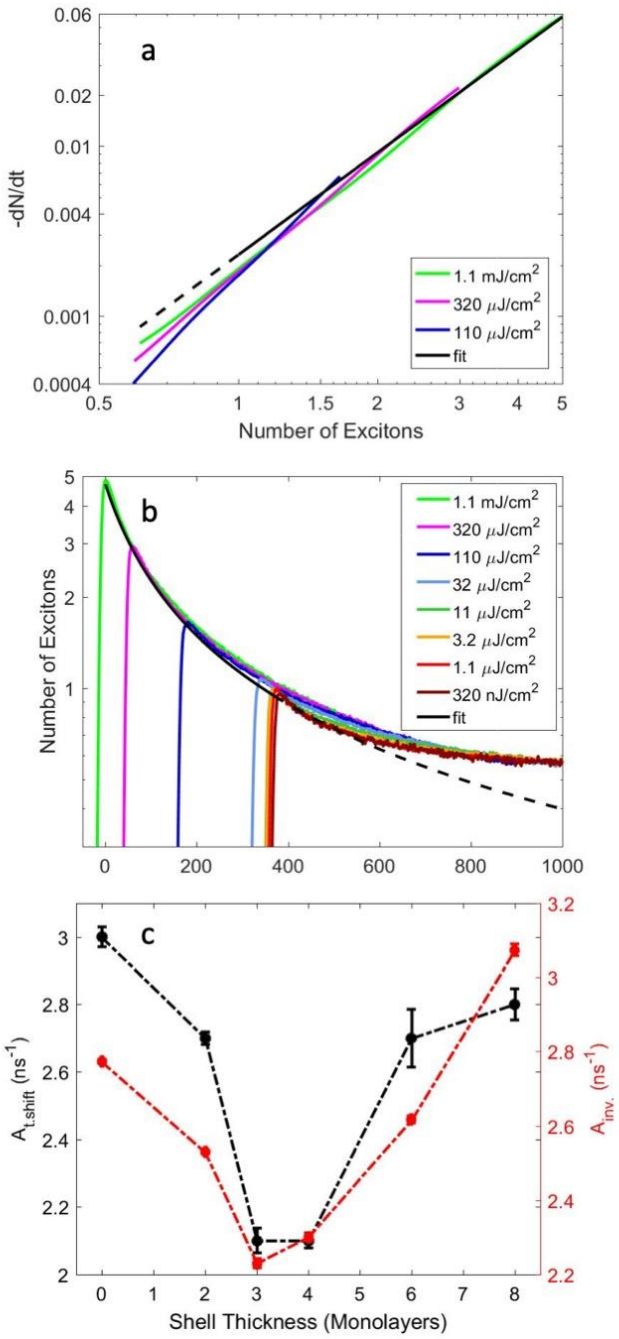

Figure 1. (a) Double-logarithmic plot of the negative rate of change in the number of excitons per nanoplatelet (NPL) following laser excitation, $-dN/dt$, as a function of the number of excitons, *N*. Data are shown for CdSe/CdS core/shell NPLs with a core thickness of 4.5 monolayers (ML) and a shell thickness of 4 ML, for three different excitation fluences. The fit is to a straight line with a slope of two, as

expected for a biexcitonic Auger recombination process. **(b)** Plot of *N* as a function of time after excitation, using the same data as in (a). Plots for different excitation fluences are shifted in time to give a universal decay curve. The fit is to Eq. (2), as expected for biexcitonic Auger recombination. **(c)** Values of the Auger recombination coefficient, *A*, obtained for NPLs with a core thickness of 4.5 ML and different shell thicknesses. Results are shown for fits of the type illustrated in (a) and (b).

The portion of the resulting universal decay curve corresponding to $N(t) > 1$ is then fit to the solution to Eq. (1):

$$N(t) = \frac{N(0)}{1+AN(0)t}. \quad (2)$$

Figure 1b shows the results of this time-shift analysis and fitting for the same data as analyzed in Figure 1a. The only adjustable fitting parameters in this fitting method are *A* and $N(0)$. Values of *A* obtained by this time-shift analysis are compared in Figure 1c to values obtained by the inversion analysis. The good agreement between the two, particularly the reproducibility of the non-monotonic dependence of Auger rate on shell thickness,[10] validates the analysis methods and shows that the values of the Auger coefficients are reliable, and are not dependent on the details of the data analysis.

Auger-Limited Relaxation Dynamics

So far, we have verified through an independent analysis method our previous claims of Auger-dominated recombination dynamics in CdSe/CdS core/shell NPLs.[10,8] We have also previously examined relaxation dynamics in CdSe (core-only) NPLs,[4] and found that they, too, were dominated by the effects of Auger recombination.[8] Specifically, reheating of carriers due to Auger

recombination results in a cooling bottleneck that determines relaxation dynamics on time scales of 10 – 100 ps.

Here, we examine whether Auger reheating still dominates the carrier relaxation dynamics for CdSe/CdS core/shell nanoplatelets. The carrier temperature, $T(t)$, is obtained from the same time-dependent PL measurements as the exciton number, $N(t)$; in this case, however, instead of integrating the PL spectra over all wavelengths, we fit the high-energy tail of the spectra to a Boltzmann distribution, with the exponent corresponding to $T(t)$.[4,20]

It can be shown that the competition between Auger reheating and electron-phonon cooling leads to the following temperature scaling for the carriers:[12]

$$T(t) - T_f \propto N(t)^2 \tag{3}$$

where T_f is the temperature reached after the carriers and lattice have reached mutual thermal equilibrium, before the slower exchange of energy between the NPL lattice and its surroundings. Figure 2 shows a plot of $T(t) - T_f$ and $CN^2(t)$ on the same graph, where *C* and T_f are constants that are adjusted to give the best overlap between the two curves at long times. It can be seen that there is a rapid, initial decrease in the temperature that is not reflected in the exciton number. At some time t_o, the two curves meet, and they overlap well for all subsequent times.

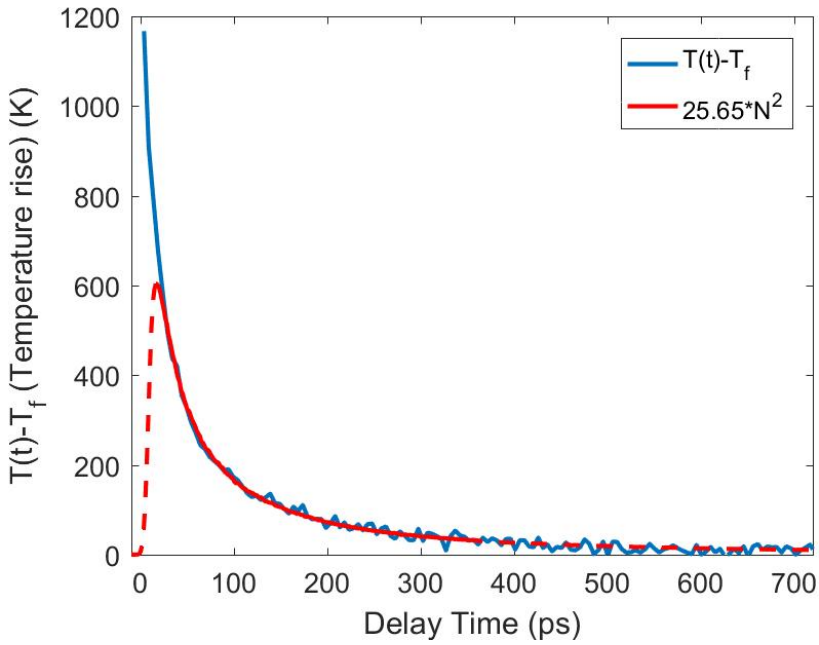

Figure 2: Average rise in the temperature of carriers inside nanoplatelets (NPLs) following laser excitation, $T(t) - T_f$, as a function of time after excitation. Data are shown for CdSe/CdS core/shell NPLs with a core thickness of 4.5 monolayers (ML) and a shell thickness of 4 ML. Also plotted is the square of the average number of excitons in each NPL, N^2, scaled by a factor to make the two curves overlap at long delay times.

We can also adopt an approach similar to the inversion analysis used above to analyze the recombination data, and make a double-logarithmic plot $T(t) - T_f$ as a function of $N(t)$; if Auger reheating is dominant, then the graph is expected to be a straight line with a slope of 2. Representative results are shown in Figure 3a. Since numerical differentiation is not required in this case, we do not smooth the data by fitting to a multiexponential function, but simply by using a moving-average filter. The expected linear relation is seen for larger values of $N(t)$. The slope of the curve increases for high $N(t)$, corresponding to the faster decay process that dominates for high exciton number, at short times after excitation.

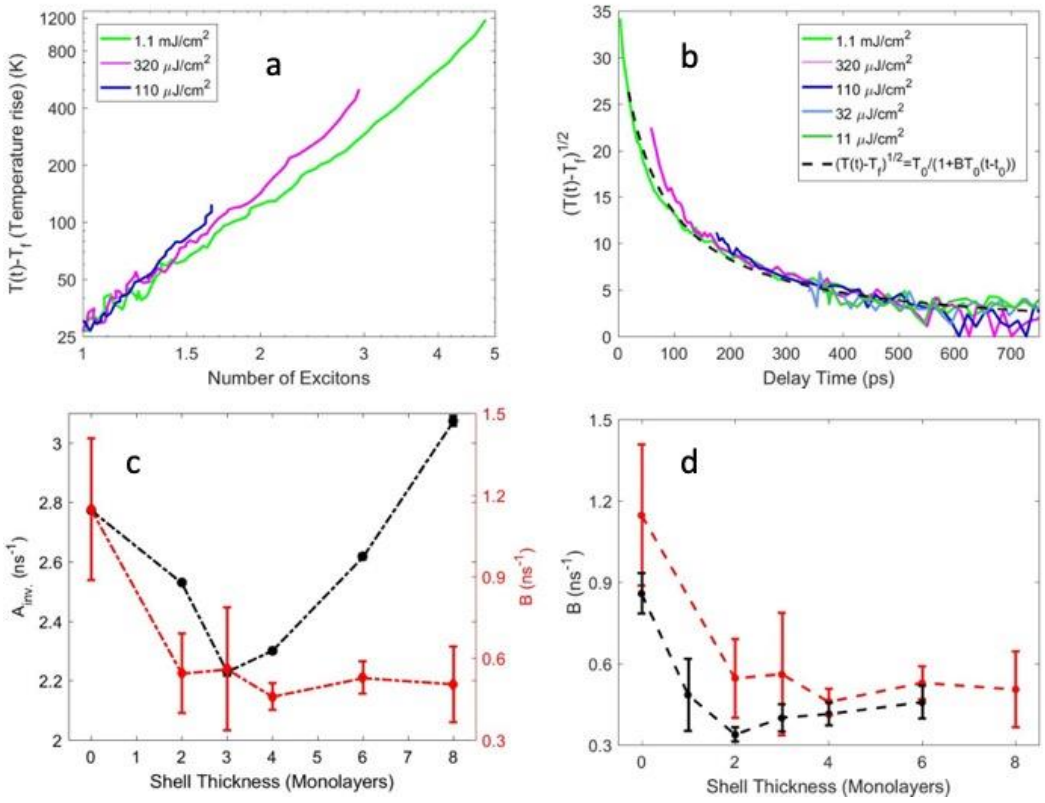

Figure 3: (a) Double-logarithmic plot of the average rise in the temperature of carriers inside nanoplatelets (NPLs) following laser excitation, $T(t) - T_f$, as a function of the number of excitons. Data are shown for CdSe/CdS core/shell NPLs with a core thickness of 4.5 monolayers (ML) and a shell thickness of 4 ML, for three different excitation fluences. **(b)** Plot of $\sqrt{T(t) - T_f}$ as a function of time after excitation, using the same data as in (a). Plots for different excitation fluences are shifted in time to give a universal relaxation curve. The fit is to Eq. (4), as expected for a cooling process that is limited by Auger reheating. **(c)** Values of the Auger recombination coefficient, *A*, obtained for NPLs with a core thickness of 4.5 ML and different shell thicknesses, compared to values for the cooling coefficient, *B*, obtained for the sample NPLs. **(d)** Values of *B* obtained for NPLs with different shell thicknesses, for core thicknesses of 4.5 ML (black points) and 5.5 ML (red points).

The fast initial decay can also be seen by applying a time-shift analysis to the relaxation data similar to that applied above to the recombination data.[8] Figure 3b shows results for this analysis, in which the data for $T(t)$ have been shifted along the time axis by the same values as the corresponding data for $N(t)$. The shifted curves can be seen to reduce to a single, universal relaxation curve for a wide range of times, *t*, but there is an initial rapid decay in each curve that is not universal. That is, the initial decay depends explicitly on the time after excitation, and not only on the instantaneous exciton number, $N(t)$.

To check whether Auger reheating indeed dominates the carrier dynamics after this initial rapid decay, we combine Eqs. (2) and (3) to give

$$\sqrt{T(t) - T_f} \propto \frac{1}{1+B \cdot T(0) \cdot (t-t_o)} \tag{4}$$

where t_o is the time at which the Auger-reheating process begins, and *B* is a constant proportional to *A*. A plot of $\sqrt{T(t) - T_f}$ as a function of *t* can therefore be fit (excluding the initial decay) to obtain *B*, as shown in Figure 3b. The values of *B* obtained from these fits can be compared to the values of *A* obtained above, within a scaling factor.

Figure 3c shows the results obtained for CdSe/CdS core/shell NPLs with a range of shell thicknesses. For shells up to 4 ML thick, *A* and *B* are in good agreement with one another. For thicker shells, *B* becomes nearly constant, instead of showing the expected increase with shell thickness. Similar results are obtained for NPLs with different core thicknesses (see Figure 3d), indicating that the assumptions underlying the analysis of the relaxation data do not hold for shell thicknesses greater than 4 ML. In other words, although recombination dynamics are dominated by biexcitonic Auger recombination for all CdSe/CdS core/shell NPLs, regardless of shell

thickness, relaxation dynamics appear to be dominated by Auger recombination only for thinner shells.

Initial Rapid Carrier Cooling

As a final stage in our analysis of carrier dynamics in core/shell NPLs, we isolate the initial, rapid decay that occurs on time scales less than 10 ps, by taking the difference between $T(t) - T_f$ and $CN^2(t)$ on Figure 2 (and similar graphs for other samples). We fit this residual to a single exponential; only the data for the highest excitation powers provided enough time points to ensure convergence of the fit. The time constants for the fast decay are 28 ± 2 ps for all samples regardless of core or shell thickness.

The measured time constant is consistent with earlier measurements in bulk CdSe,[21] where cooling was attributed to generation of LO phonons by hot carriers, and the cooling rate was limited by decay of the LO-phonon population.[22,23] This model is consistent with the insensitivity of the initial decay to shell thickness, since the cooling rate depends only on the LO-phonon lifetime, and is largely insensitive to the electron-phonon coupling strength and (unlike Auger recombination)[10,24] to details of the carrier wavefunctions. This cooling stage, where the rate is limited by LO-phonon decay, is expected to occur only after a large LO-phonon population has been created, and is thus expected to be preceded by an even faster decay, on single-picosecond time scales, whose rate is determined by the electron-phonon coupling strength;[25] this ultrafast cooling has previously been observed using photoemission spectroscopy, but is outside the time resolution of our experiment.

Discussion

We have shown that Auger processes dominate the recombination dynamics of CdSe/CdS core/shell nanoplatelets for all shell thicknesses and dominate relaxation dynamics for shell thicknesses up to 4 monolayers. For thicker shells, the time dependence of the carrier temperatures has a similar time dependence as for thinner shells, but analysis based on a simple model of Auger reheating gives Auger recombination rates that are inconsistent with those obtained by analyzing the recombination dynamics. The reason for the breakdown of the simple model for thicker shells is not yet clear, but may be related to the reduced overlap between the envelope wavefunctions for the electron (which extends over the entire NPL structure) and the hole (which is confined to the CdSe core). Microscopic modeling will be required to resolve the underlying mechanisms responsible for the change in relaxation dynamics with the change in shell thickness.

We have also observed, for all CdSe/CdS core/shell NPLs studied, an initial, rapid carrier relaxation that is not limited by Auger reheating. The time constant for this relaxation is approximately 28 ps, regardless of shell thickness, consistent with an electron-phonon cooling process whose rate is limited by the LO-phonon lifetime. However, the dynamic range of the data corresponding to this initial decay was limited by the time resolution of the streak-camera measurements that we performed. Further insight into this process will require time-resolved measurements with resolution on the order of 100 fs, such as PL upconversion spectroscopy[26] or transient-absorption spectroscopy.7,[27]

The results presented here complement and extend previous measurements of carrier dynamics in colloidal semiconductor NPLs,[6] showing in particular how these dynamics are qualitatively different from those in colloidal semiconductor quantum dots. This crucial role of dimensionality is expected to hold for other quantum-confined nanomaterials. The results obtained here thus have the potential to provide broader insight into carrier recombination and relaxation in a wide array

of two-dimensional nanostructures, including perovskite nanoplatelets[28,29,30] and transition metal dichalcogenides.[31,32]

AUTHOR INFORMATION

Corresponding Author

*mpelton@umbc.edu

Present Addresses

†Los Alamos National Laboratory, Los Alamos, NM 87545, U.S.A.

Author Contributions

M.P. conceived the experiment, performed streak-camera measurements, and prepared the manuscript. Y.W. analyzed the data. I.F. synthesized nanoplatelet samples. D.T. supervised nanoplatelet synthesis. S.O. and M.P. supervised data analysis. All authors contributed to discussions.

ACKNOWLEDGMENTS

We thank Richard Schaller for assistance with the streak-camera measurements, and Alan Bristow for helpful discussions. This work was performed, in part, at the Center for Nanoscale Materials, a U.S. Department of Energy Office of Science User Facility under Contract No. DE-AC02-06CH11357. Work at The University of British Columbia was funded by the Natural Sciences and Engineering Research Council of Canada. Y.W. acknowledges support from the Chinese Scholarship Council (CSC). I.F. and D.V.T. acknowledge support from the National Science Foundation under award DMR-1629601.

REFERENCES

[1] Pietryga, J. M.; Park, Y.-S.; Lim, J.; Fidler, A. F.; Bae, W. K.; Brovelli, S.; Klimov, V. I. Spectroscopic and Device Aspects of Nanocrystal Quantum Dots. *Chem. Rev.* **2016**, *116*, 10513-10622.

[2] Harris, R. D.; Homan, S. B.; Kodaimati, M.; He, C.; Nepomnyashchii, A. B.; Swenson, N. K.; Lian, S.; Calzada, R.; Weiss, E. A. Electronic Processes within Quantum Dot – Molecule Complexes. *Chem. Rev.* **2016**, 116, 12865-12919.

[3] Nozik, A. J. Quantum Dot Solar Cells. *Physica E* **2002**, 14, 115-120.

[4] Nozik, A. J. Spectroscopy and Hot Electron Relaxation Dynamics in Semiconductor Quantum Wells and Quantum Dots. *Annu. Rev. Phys. Chem.* **2001**, 52, 193-231.

[5] Lhuillier, E.; Pedetti, S.; Ithurria, S.; Nadal, B.; Heuclin, H.; Dubertret, B. Two-Dimensional Colloidal Metal Chalcogenides Semiconductors: Synthesis, Spectroscopy, and Applications. *Acc. Chem. Res.* **2015**, 48, 22-30.

[6] Pelton, M. Carrier Dynamics, Optical Gain, and Lasing with Colloidal Quantum Wells. *J. Phys. Chem. C* **122**, 10659 (2018).

[7] Pelton, M.; Ithurria, S.; Schaller, R.D.; Dolzhinkov, D.S.; Talapin, D.V. Carrier Cooling in Colloidal Quantum Wells. *Nano Lett.* **2012**, 12, 6158-6163.

[8] Baghani, E.; O'Leary, S.K.; Fedin, I.; Talapin, D. V.; Pelton, M. Auger-Limited Carrier Recombination and Relaxation in CdSe Colloidal Quantum Wells. *J. Phys. Chem. Lett.* **2015**, 6, 1032-1036.

[9] Klimov, V. I.; McBranch, D. W. Femtosecond 1*P*-to-1*S* Electron Relaxation in Strongly Confined Semiconductor Nanocrystals. *Phys. Rev. Lett.* **1998**, *80*, 4028-4031.

[10] Pelton, M.; Andrews, J. J.; Fedin, I.; Talapin, D. V.; Leng, H.; O'Leary, S. K. Nonmonotonic Dependence of Auger Recombination Rate on Shell Thickness for CdSe/CdS Core/Shell Nanoplatelets. *Nano Lett.* **2017**, 6900-6906.

[11] Kunneman, L. T.; Tessier, M. D.; Heuclin, H.; Dubertret, B.; Aulin, Y. V.; Grozema, F. C.; Schins, J. M.; Siebbeles, L. D. A. Bimolecular Auger Recombination of Electron-Hole Pairs in Two-Dimensional CdSe and CdSe/CdZnS Core/Shell Nanoplatelets. *J. Phys. Chem. Lett.* **2013**, 4, 3574-3578.

[12] Borri, P.; Ceccherini, S.; Gurioli, M.; Bogani, F. Auger Heating of Carriers in GaAs/AlAs Heterostructures. *Solid State Comm.* **1997**, 103, 77-81.

[13] Achermann, M.; Bartko, A. P.; Hollingsworth, J. A.; Klimov, V. I. The Effect of Auger Heating on Intraband Carrier Relaxation in Semiconductor Quantum Rods. *Nat. Phys*. **2006**, 2, 557-561.

[14] Li, M.; Bhaumik, S.; Goh, T. W.; Kumar, M. S.; Yantara, N.; Grätzel, M.; Mhaisalkar, S.; Mathews, N.; Sum, T. C. Slow Cooling and Highly Efficient Extraction of Hot Carriers in Colloidal Perovskite Nanocrystals. *Nat. Comms.* **2017**, 14350 (2017)

[15] Fu, J.; Xu, Q.; Han, G.; Wu, B.; Huan, C. H. A.; Look, M. L.; Sum, T. C. Hot Carrier Cooling Mechanisms in Halide Perovskites. *Nat. Comms.* **2017**, 8, 1300 (2017).

[16] Papagiorgis, P.; Protesescu, L.; Kovalenko, M. V.; Othonos, A.; Itskos, G. Long-Lived Hot Carriers in Formamidium Lead Iodide Nanocrystals. *J. Phys. Chem. C* **2017**, 121, 12434-12440.

[17] Barzykin, A.V.; Tachiya, M. Stochastic Models of Charge Carrier Dynamics in Semiconducting Nanosystems. *J. Phys. – Cond. Matt.* **2007**, 19, 065105.

[18] Senty, T. R.; Cushing, S. K.; Wang, C.; Matranga, C.; Bristow, A. D. Inverting Transient Absorption Data to Determine Transfer Rates in Quantum Dot – TiO_2 Heterostructures. *J. Phys. Chem. C* **2015**, 119, 6337-6343.

[19] Ithurria, S.; Talapin, D.V. Colloidal Atomic Layer Deposition (c-ALD) using Self-Limiting Reactions at Nanocrystal Surface Coupled to Phase Transfer between Polar and Nonpolar Media. *J. Am. Chem. Soc.* **2012**, 134, 18585-15890.

[20] Leo, K.; Rühle, W. W.; Ploog, K. Hot-Carrier Energy-Loss Rates in GaAs/$Al_xGa_{1-x}As$ Quantum Wells. *Phys. Rev. B* **1988**, *38*, 1947-1957.

[21] Junnarkar, M. R.; Alfano, R. R. Photogenerated High-Density Electron-Hole Plasma Energy Relaxation and Experimental Evidence for Rapid Expansion of the Electron-Hole Plasma in CdSe. *Phys. Rev. B* **1986**, *34*, 7045-7062.

[22] van Driel, H. M. Influence of Hot Phonons on Energy Relaxation of High-Density Carriers in Germanium. *Phys. Rev. B* **1979**, 19, 5928-5932.

[23] Vengurlekar, A. S.; Prabhu, S. S.; Roy, S. K.; Shah, J. Large Reduction in Hot-Carrier Energy-Loss Rates in CdSe Caused by Nonequilibrium Optical Phonons. *Phys. Rev. B* **1994**, *50*, 15461-15464.

[24] Vaxenburg, R.; Rodina, A.; Lifshitz, E.; Efros, Al. L. Biexcitonic Auger Recombination in CdSe/CdS Core/Shell Semiconductor Nanocrystals. *Nano Lett*. **2016**, 16, 2503-2511.

[25] Sippel, P.; Albrecht, W.; van der Bok, J. C.; Van Dijk-Moes, R. J. A.; Hannappel, T.; Eichberger, R.; Vanmaekelbergh, D. Femtosecond Cooling of Hot Electrons in CdSe Quantum-Well Platelets. *Nano Lett.* **2015**, 15, 2409-2416.

[26] Underwood, D. F.; Kippeny, T.; Rosenthal, S. J. Ultrafast Carrier Dynamics in CdSe Nanocyrstals Determined by Fluorescence Upconversion Spectroscopy. *J. Phys. Chem. B* **2001**, 105, 436-443.

[27] Kunneman, L. T.; Schins, J. M.; Pedetti, S.; Heuclin, H.; Grozema, F. C.; Houtepen, A. J.; Dubertret, B.; Siebbeles, L. D. A. Nature and Decay Pathways of Photoexcited States in CdSe and CdSe/CdS Nanoplatelets. *Nano Lett.* **2014**, 14, 7039-7045.

[28] Tyagi, P.; Arveson, S. M.; Tisdale, W. A. Colloidal Organohalide Perovskite Nanoplatelets Exhibiting Quantum Confinement. *J. Phys. Chem. Lett.* **2015**, *6*, 1911-1916.

[29] Bekenstein, Y.; Koscher, B. A.; Eaton, S. W.; Yang, P.; Alivisatos, A. P. Highly Luminescent Colloidal Nanoplatelets of Perovskite Cesium Lead Halide and Their Oriented Assemblies. *J. Am. Chem. Soc.* **2015**, *137*, 16008-16011.

[30] Akkerman, Q. A.; Motti, S. G.; Kandada, A. R. S.; Mosconi, E.; D'Innocenzo, V.; Bertoni, G.; Marras, S.; Kamino, B. A.; Miranda, L.; De Angelis, F.; *et al*. Solution Synthesis Approach to Colloidal Cesium Lead Halide Perovskite Nanoplatelets with Monolayer-Level Thickness Control. *J. Am. Chem. Soc.* **2016**, *138*, 1010-1016.

[31] Wang, Q. H.; Kalantar-Zadeh, K.; Kis, A.; Coleman, J. N.; Strano, M. S. Electronics and Optoelectronics of Two-Dimensional Transition Metal Dichalcogenides. *Nat. Nano.* **2012**, 7, 699-712.

[32] Novoselov, K. S.; Mishchenko, A.; Carvalho, A.; Castro Neto, A. H. 2D Materials and van der Waals Heterostructures. *Science* **2016**, *353*, aac9439.